journal

J. Am. Ceram. Soc., 1–6 (2016)
DOI: 10.1111/jace.14248

Suppression of Silver Diffusion in Borosilicate Glass-Based Low-Temperature Cofired Ceramics by Copper Oxide Addition

Mingsheng Ma, Zhifu Liu,† Faqiang Zhang, Feng Liu, and Yongxiang Li†

The Key Laboratory of Inorganic Functional Materials and Devices, Shanghai Institute of Ceramics, Chinese Academy of Sciences, Shanghai 200050, China

The silver diffusion behavior in the low-temperature cofired ceramic (LTCC) comprising of borosilicate glass and alumina was investigated in this work. Transmission electron microscope (TEM) analysis revealed that silver ions diffused into LTCC materials through the glass phase. The addition of copper oxide in the LTCC materials can suppress the silver diffusion during the sintering process because of the enhanced crystallization of borosilicate glass, which leads to the quick increase in glass viscosity and retards the silver diffusion. Thermal dynamic analysis confirmed that the diffusion coefficient of silver in the copper-oxide-modified LTCC materials was largely reduced.

Keywords: *borosilicate glass; alumina; LTCC; silver/silver compounds; diffusion/diffusivity*

I. Introduction

Since no atmosphere control is needed during silver cofiring and relatively low cost, silver is a widely used metal electrode in the low-temperature cofired ceramic (LTCC) components/devices manufacturing.[1–3] However, due to the mismatched densification kinetics and mechanism between silver and LTCC ceramics, some undesirable phenomena including silver diffusion, delamination, cracks, and camber might occur during cofiring process.[4–6] Silver diffusion is one of the key issues because it could lead to not only the color stain of the sample appearance but also the increase in leakage current, the decrease in insulation resistance, and eventually affect the electrical properties and reliability of the LTCC modules.[7]

Large amount of low melting point frit in LTCC materials is the main reason of the silver diffusion at the sliver/LTCC interface. Silver could diffuse into the glass phase of LTCC material, and glass may also filter into the electrode layer at higher sintering temperature.[8] Ag_2O is the most possible intermediate form of silver at the interface.[9] Jean et al. reported that interfacial reactions between silver and the glass matrix could cause an interfacial reaction zone at silver/LTCC interface, where the dissolved Ag^+ ion resulting from the oxidation of silver played a key role.[9] They also presented that the oxidation of Ag to Ag_2O could be suppressed by cofiring in reducing atmosphere.

It was considered that the driving force of the silver diffusion is related to the viscous flow of glassy phase during cofiring process.[10,11] Efforts have been therefore made to increase the viscosity of glass phase by adjusting the composition of LTCC materials.[12] However, there is no clear image about the silver diffusion mechanism yet. Therefore, further study is needed to understand deeply the behavior of silver at the silver/LTCC interface during the cofiring process.

The study on chemical compatibility between silver electrodes and binary-oxide compounds provided a good reference for the choice of LTCC compositions.[13] Copper oxide (CuO) is considered to be one of the ideal choices for its less reactive toward silver.[14] Furthermore, CuO has been reported as a good sintering aid for lowering the sintering temperature and improving the microwave dielectric properties of LTCC materials.[15] But, few studies have been done on the effects of CuO additive to LTCCs on silver diffusion phenomenon. In this work, the effective suppression of the silver diffusion at the silver/LTCC interface by CuO addition in the borosilicate glass-based LTCC materials is reported. The mechanism is discussed by comparing the microstructure and silver diffusion behavior of the CuO-modified and unmodified LTCC materials.

II. Experimental Procedure

The LTCC material used in this work was composed of borosilicate glass and alumina. The compositions of borosilicate glass powders without and with the addition of CuO were 25 CaO–15 Al_2O_3–20 B_2O_3–40 SiO_2 (wt%, CABS1) and 25 CaO–15 Al_2O_3–19 B_2O_3–40 SiO_2–1 CuO (wt%, CABS2), respectively. A commercially available alumina powder (Zibo Xinmeiyu Alumina Co., Ltd. Shandong, China) with a mean diameter of ~1 μm was used as filler. Two series of LTCC green tapes with a fixed amount of alumina was used in this work. 52 CABS1–48 Al_2O_3 (wt%, LTCC1) and 52 CABS2–48 Al_2O_3 (wt%, LTCC2) were tape-casted. Details on glass powders and LTCC green tapes preparation can be found in our previous papers.[16,17] Commercial silver paste (Dupont 6142D, Santa Barbara, CA) was used for cofiring investigation. Twenty layers of green tapes with printed silver patterns were laminated at 70°C under a pressure of 48 MPa for 10 min in an isostatic laminator (Pacific Trinetics Corporation LT08001, Los Alamitos, CA). The laminates were cut as chips with a size of 20 mm × 20 mm and debindered at a heating rate of 1.5°C/min from room temperature to 450°C and held for 2 h. And then, the samples were sintered at temperatures between 850°C and 925°C for 30 min by a heating rate of 10°C/min.

Phase identification was performed by X-ray diffraction analysis (XRD, Rigaku D/MAX 2550V, Tokyo, Japan). The thermal behavior of the glasses was performed by differential thermal analysis (DTA, Netzsch STA 449C, Selb, Germany) with a heating rate of 10°C/min in air, and alumina was used as the reference material. The microstructures of the samples were examined by transmission electron microscope (TEM, JEOL JEM-2100F, Tokyo, Japan). The silver concentration in LTCC near the silver electrode/LTCC interface was calculated using the results of energy dispersion spectroscopy (EDS) equipped on the scanning electron microscope (SEM, JEOL JXA-8100). The valent states of the elements in LTCC

R. Bordia—contributing editor

Manuscript No. 37519. Received September 16, 2015; approved March 7, 2016.
†Authors to whom correspondence should be addressed. e-mails: yxli@mail.sic.ac.cn and liuzf@mail.sic.ac.cn

materials were analyzed by X-ray photoelectron spectroscopy (XPS, ESCALAB 250, Thermo Fisher Scientific, Waltham, US). The dielectric properties were measured by an impedance analyzer (Wayne-Kerr, 6500B, West Sussex, UK) at 1 MHz.

III. Results and Discussion

Yellow halo stain around cofired silver external conductors can be observed from LTCC1 sintered at temperatures between 850°C and 925°C for 30 min, whereas the LTCC2 with CuO addition sintered at the same condition shows no yellow stain, as shown in the insert of Fig. 1(a). The yellow color around silver electrode in LTCC1 was related to the silver diffusion.[5,8] Figure 1(a) also shows the XPS spectra of the small areas near Ag electrode of both LTCC1 and LTCC2 sintered at 875°C for 30 min. As expected, the peaks of Ca, Al, Si, B, and O elements are determined in both samples. The difference between the two spectra is that Ag 3*d* peaks are detected from the yellow area in LTCC1. However, there is no any Ag peak in the spectra of LTCC2. This indicates that the addition of CuO into the glass could prevent silver diffusion in LTCC2. In addition, a weak Cu $2P_{3/2}$ peak is observed in LTCC2. The binding energy of the Cu $2P_{3/2}$ peak is 933.8 eV, which falls in the Cu^{2+} binding energy range 933.2–934.1 eV for CuO.[18] Figure 1(b) shows that the binding energy of Ag3$d_{5/2}$ peak in LTCC1 is 368.1 eV. Binding energies given in Table I for the Ag 3$d_{5/2}$ peak of Ag, Ag_2O, and AgO are 368.2, 367.8, and 367.4 eV, respectively.[19,20] The Ag $3d_{5/2}$ binding energy of 368.1 eV obtained in this work are between that of Ag and Ag_2O. This implies that Ag^+ may be coexistence with Ag^0 in LTCC1. It is well accepted that silver diffuses in LTCC materials through glass network with Ag^+ form. The observed Ag^0 might result from the partial precipitation of Ag^+ from glass network at the high sintering temperature.

The XPS results indicated that the presence of the yellow stain is related to the diffused sliver in the LTCC1. Masuko had reported that the coloration would occur when Ag^+ ions transform into Ag colloids during the cofiring of CABS glass and silver.[21] Ag colloids usually exhibit a yellow color, because the Ag colloidal nanoparticles absorb light energy from the visible spectrum typically at a wavelength around 400 nm.[22] The yellow color is the complement of the absorbed wavelength (purple and yellow are the complementary colors).

To find out the effect of CuO addition on Ag diffusion behavior of borosilicate glass/Al_2O_3-based LTCC materials, the Ag content in LTCC material near the Ag/LTCC interface was analyzed. Figure 2(a) shows the concentration profile of silver from silver internal conductors layer to LTCC1 sintered at 850°C, 875°C, 900°C, and 925°C. The concentration of silver in LTCC materials can be calculated as follows:[8]

$$\frac{C_{Ag}(x,t)}{C_{Ag}} = 1 - erf\left[\frac{x}{2\sqrt{D_{Ag}t}}\right] \quad (1)$$

where C_{Ag} is equal to 100% for silver internal conductor, $C_{Ag}(x,t)$ is the concentration of silver measured at distance x from the interface of silver internal conductor for a given period of time (t), D_{Ag} is the diffusion coefficient of silver, and the *erf* in Eq. (1) is error function. The ratio of $C_{Ag}(x,t)/C_{Ag}$ was obtained from EDS measurements. The average diffusion coefficients of silver in LTCC1 determined by Eq. (1) are 2.72×10^{-13} cm^2/s at 850°C, 3.57×10^{-13} cm^2/s at 875°C, 5.46×10^{-13} cm^2/s at 900°C, and 8.15×10^{-13} cm^2/s at 925°C. These values are comparable to those previously reported in the alumina-filled glass LTCC system.[8] The average diffusion coefficients of silver in LTCC2 are 1.04×10^{-13} cm^2/s at 850°C, 1.89×10^{-13} cm^2/s at 875°C, 2.92×10^{-13} cm^2/s at 900°C, and 3.78×10^{-13} cm^2/s at 925°C, as illustrated in Fig. 2(b). It is found that the average diffusion coefficients of silver in LTCC2 are much less than those in LTCC1.

Figure 3 presents the Arrhenius plots obtained from the average diffusion coefficients of silver at all temperatures. The activation energy of silver diffusion (Q_d) can be calculated from Arrhenius equation:

$$D_{Ag} = D_0 \exp\left(-\frac{Q_d}{RT}\right) \quad (2)$$

where D_0 is a pre-exponential factor, R is the gas constant, 8.31 $J\cdot(mol\cdot K)^{-1}$. The Q_d values of LTCC1 and LTCC2

Table I. Binding Energies for the Ag $3d_{5/2}$ peak of Ag, Ag_2O, and AgO

	Binding energy (eV)	
Materials	Ag $3d_{5/2}$	O *1s*
Ag powder	368.2	531.0
Ag_2O	367.8	529.2
AgO	367.4	528.6
This work	368.1	532.0

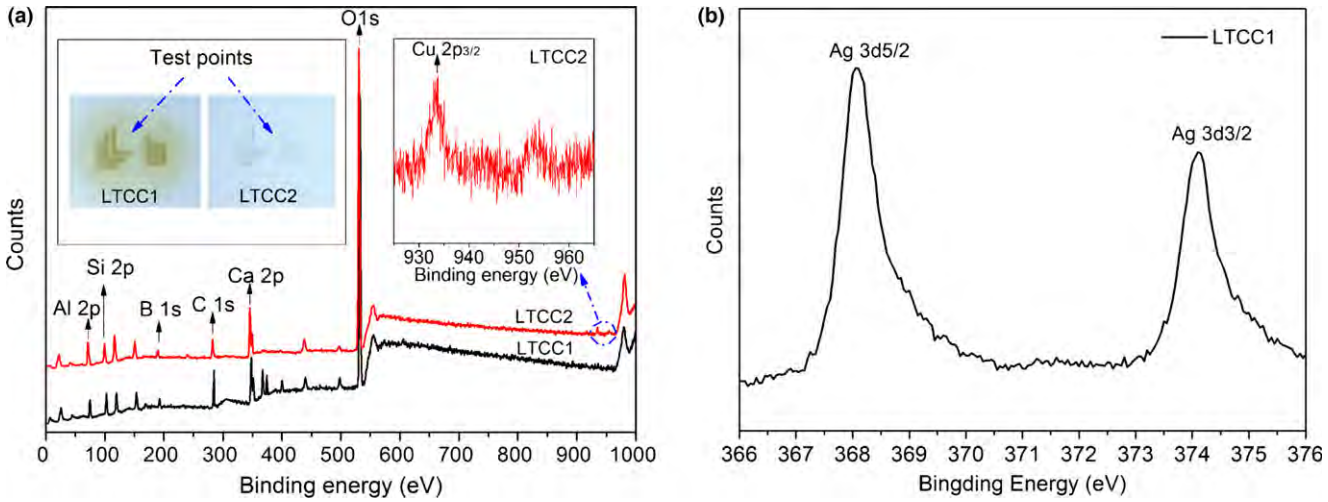

Fig. 1. (a) The XPS spectra of LTCC1 and LTCC2 tested on the same position of both samples. Inserts show the cofired samples pictures. (b) The magnification of XPS near 367 eV in LTCC1.

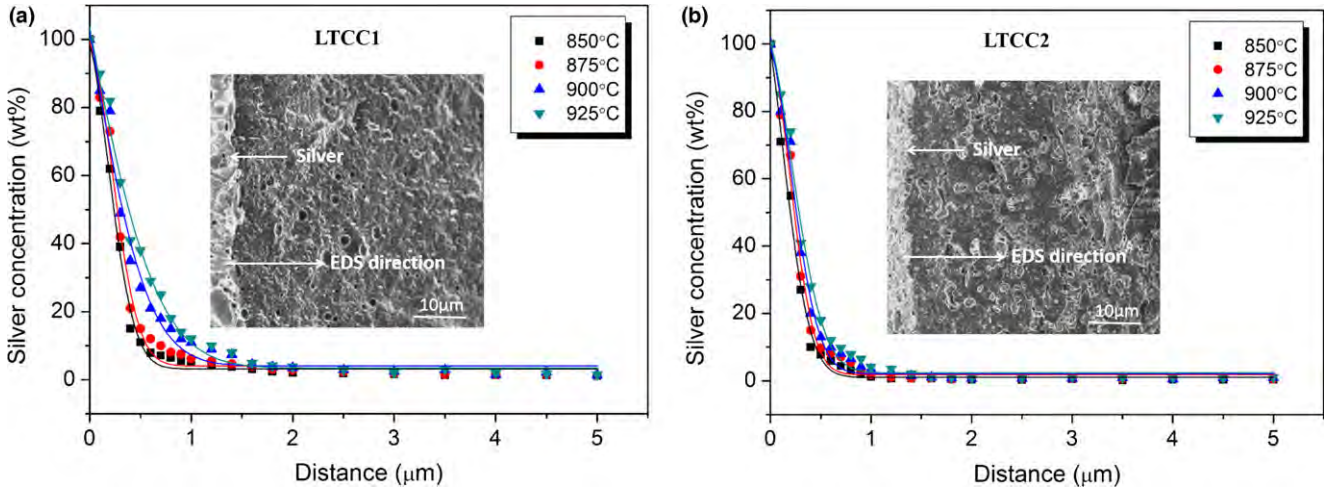

Fig. 2. The concentration profiles of silver from silver internal conductors layer to LTCC1 (a) and LTCC2 (b), sintered at 850°C, 875°C, 900°C, and 925°C for 30 min.

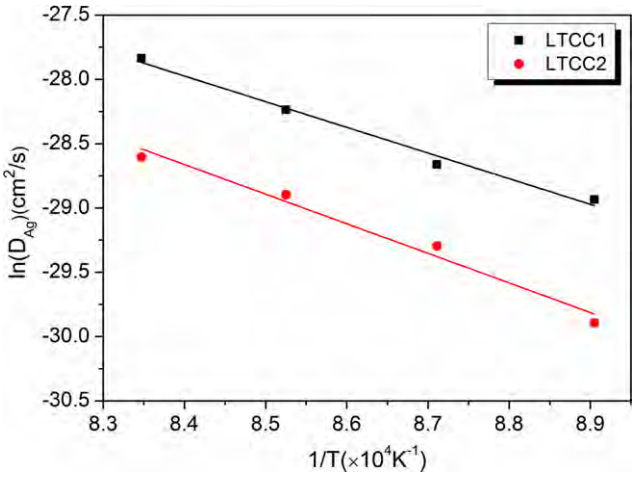

Fig. 3. Logarithm of the diffusion coefficient of silver [$\ln(D_{Ag})$] as a function of reciprocal temperature ($1/T$).

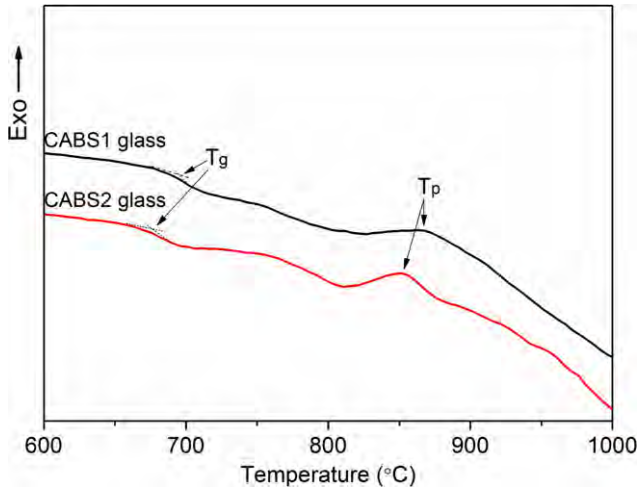

Fig. 4. DTA curves of CABS1 and CABS2 glass.

determined from the slops of the linear fit lines are 165.3 and 191.1 kJ/mol, respectively. The larger Q_d value of LTCC2 is probably due to the change in microstructure in the LTCC2 induced by CuO addition. It is suggested that silver diffusion would more preferably happen in LTCC1. In addition, the Q_d values of LTCC1 and LTCC2 are higher than the previous reports,[9,12] which is probably due to the different glass system and alumina content used in this study. The rigid alumina content (48 wt%) here is higher than that of previous reports (5–40 wt%) and the alumina particles could act as barrier retarding silver diffusion.[12]

To further confirm the effect of CuO addition on the LTCC materials, thermal analysis, phase identification, dielectric properties measurements and microstructure observations have been carried out. Figure 4 represents the DTA curves of CABS1 and CABS2 glass. It was found that the glass-transition temperatures (T_g) of CABS1 and CABS2 glass were about 690°C and 675°C, respectively. Exothermic peaks (T_p) were observed at the temperatures of 869°C and 852°C, which were related to the crystallization of the CABS1 and CABS2 glass, respectively. These results suggest that the addition of CuO in CABS2 glass lowers the T_g and T_p, compared to those of CABS1 glass. As a glass network modifier, CuO might partially interrupt the borosilicate glass network structure and therefore decrease the activation energy for crystallization. As a result, LTCC2 crystallized at lower temperature than LTCC1 under the same sintering procedure.

The XRD patterns of CABS1 and CABS2 glass sintered at 825°C–925°C for 30 min are shown in Fig. 5. It can be seen that CABS1 and CABS2 glass begin to crystallize at 850°C, which is consistent with the DTA results. The major XRD peaks are identified as anorthite ($CaAl_2Si_2O_8$) with a triclinic unit cell (JCPDS card No. 41-1486, a = 8.176 Å, b = 12.872 Å, c = 14.183 Å, α = 93.172°, β = 115.911°, γ = 91.199°, space group $P1$). The peak of anorthite (0 0 4) appears from 850°C in both CABS1 and CABS2, and the peaks become much stronger as the temperature increasing in the both glass samples. However, the other XRD peaks of anorthite (0 −4 2), (−2 4 2), and (2 −4 2) could be observed in CABS2 glass, which is much more obvious than CABS1 glass. This suggests that the crystallization of CABS glass has been enhanced by the CuO addition.

Since the CABS1 and CABS2 glass would melt at 850°C or higher, the samples sintered at 750°C–825°C for 30 min were used for dielectric properties measurements, as shown in Table II. It can be seen that CABS1 and CABS2 glass showed a low dielectric constant (ε_r) within the range of 3.1–4.3. Since the sintering shrinkage of CABS1 and CABS2 glass just started from 750°C, the rather lower dielectric constant for the samples sintered at 750°C should be attributed to the high porosity inside the samples. The dielectric constants in both glass showed an increasing trend with sintering temperature increasing from 750°C to 825°C, and the dielectric loss ($\tan\delta$) showed an opposite trend, which could be

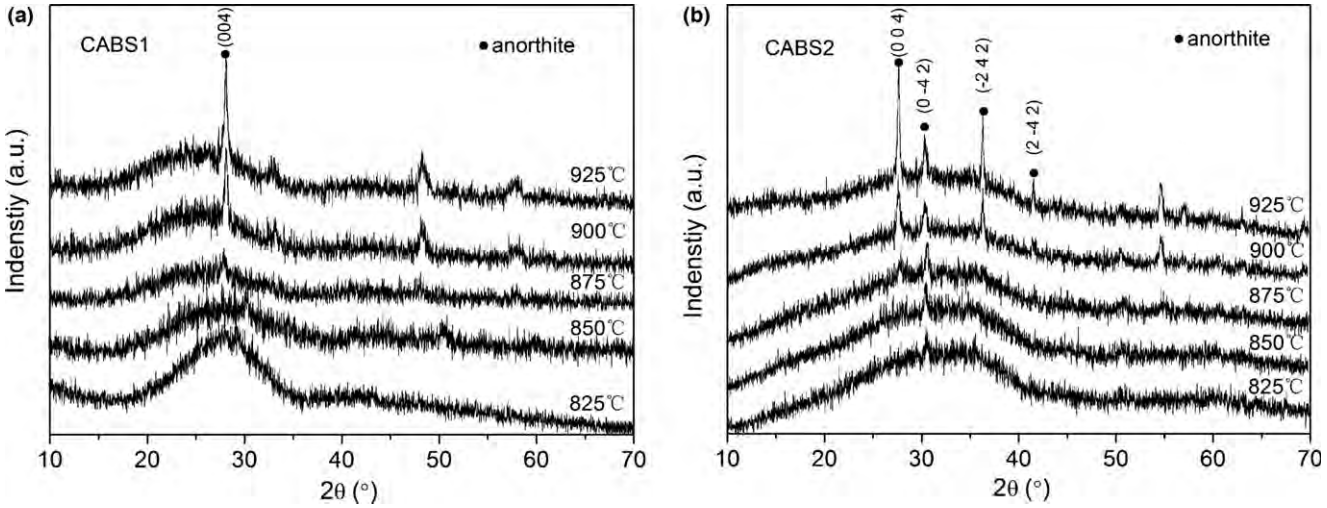

Fig. 5. XRD patterns of (a) CABS1 and (b) CABS2 sintered at 825°C–925°C for 30 min.

Table II. The Dielectric Properties of CABS1 and CABS2 (1 MHz)

Samples	Dielectric properties	750°C	775°C	800°C	825°C
CABS1	ε_r	3.11	3.98	4.12	4.23
	tanδ	0.27	0.09	0.08	0.11
CABS2	ε_r	3.29	4.07	4.20	4.27
	tanδ	0.13	0.04	0.07	0.15

due to the increased density of the glass matrix with the increase in the sintering temperature.

Due to the densification temperature range for LTCC1 and LTCC2 was 850°C–925°C, the samples for XRD analysis and dielectric properties measurements were sintered at this temperature range. Figure 6 shows the XRD patterns of LTCC1 and LTCC2 sintered at temperatures between 850°C and 925°C for 30 min. The Al_2O_3 peaks can be observed from all XRD patterns and accompanied by the anorthite phase with different intensity. It has been reported that the pronounced anorthite crystallization is accompanied by significant dissolution of alumina in the CABS glass.[23] The anorthite formation occurs as a result of two solid phase-boundary reactions involving alumina dissolution and a reduction in the amount of residual glass phase. Thus, the XRD peaks of anorthite in LTCC1 and LTCC2 were more obvious than those of CABS1 and CABS2 glass. In addition, the XRD peak intensity of the anorthite phase from LTCC2 is much stronger than that of LTCC1. Semiquantitative calculations of XRD data using software MDI JADE 5.0 showed that the crystallization amount of anorthite in LTCC2 were 1.53, 2.61, 2.97, and 3.12 times than that in LTCC1 for the samples sintered at 850°C, 875°C, 900°C, and 925°C, respectively. These results further suggest that the addition of CuO enhanced the crystallization of the glass matrix.

Table III showed the dielectric properties versus the sintered temperature of LTCC1 and LTCC2. The dielectric constants of both LTCC1 and LTCC2 increase slightly with the increase in sintering temperature from 850°C to 900°C. However, the trends of dielectric loss of LTCC1 and LTCC2 are different from that of dielectric constant. LTCC2 shows larger dielectric constant and lower dielectric loss than LTCC1 at the same sintering condition. The lower dielectric loss of LTCC 2 should be resulted from the higher degree of crystallinity of CABS2 glass induced by CuO addition.

The microstructure of LTCC1 with yellow stain and LTCC2 around the silver external conductor was analyzed

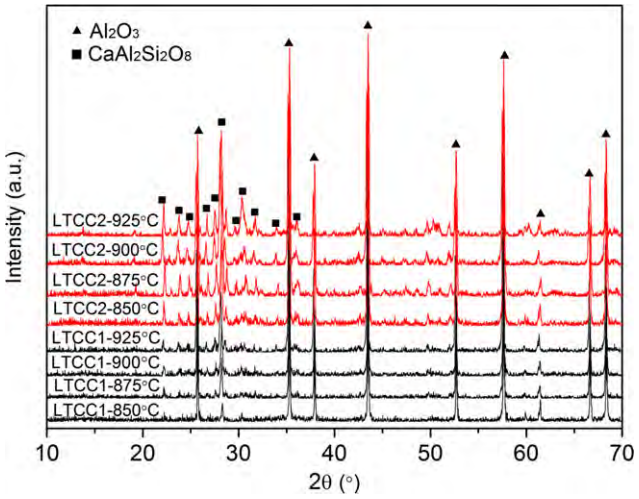

Fig. 6. XRD patterns of LTCC1 and LTCC2 without silver cofiring, sintered at temperatures between 850°C and 925°C for 30 min.

Table III. The Dielectric Properties of LTCC1 and LTCC2 (1 MHz)

Samples	Dielectric properties	850°C	875°C	900°C	925°C
LTCC1	ε_r	6.84	6.98	7.07	7.01
	tanδ	0.008	0.005	0.003	0.006
LTCC2	ε_r	6.92	7.15	7.43	7.31
	tanδ	0.006	0.003	0.002	0.002

by transmission electron microscopy (TEM). From the bright field images of LTCC1 as shown in Figs. 7(a) and (b), it is clear that the Al_2O_3 grains are partially surrounded by the glass matrix and some nanocrystallized phases, which are pointed out by the circles. The nanocrystallized phases are very likely to be anorthite according to the XRD analysis. This was confirmed by the selected-area electron-diffraction (SAED) patterns, as shown in Fig. 7(b). It is known that the SAED patterns of pure glass are halos. However, the SAED patterns extracting from these nanocrystallized phases showed that amorphous halos were accompanied by crystal electron-diffraction spots. This revealed that there were crystallized phases formed in the glass matrix. Figs. 7(d)–(f) show typical bright field images of the sample LTCC2. Since the crystallinity of LTCC2 was much better than that of LTCC1,

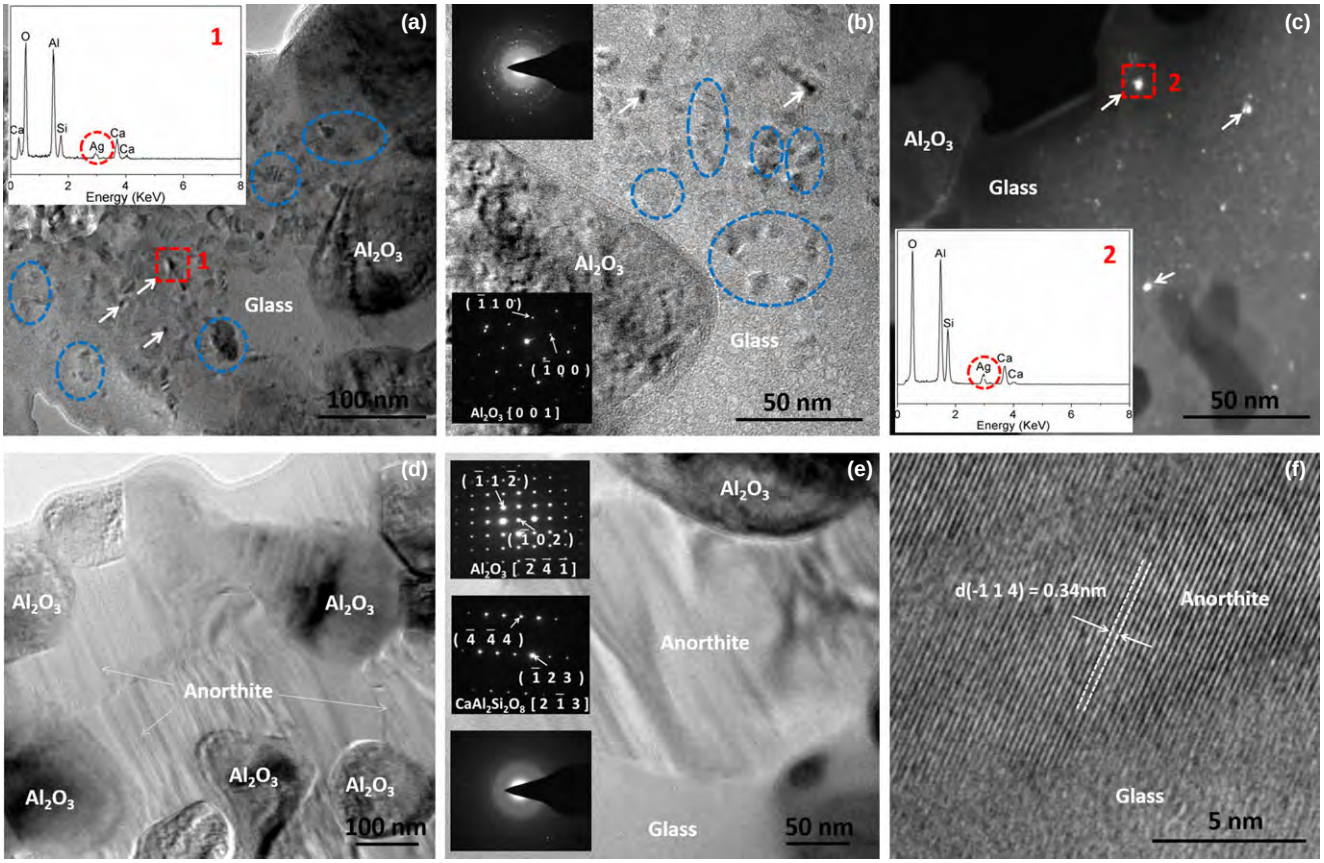

Fig. 7. TEM images of (a)–(c) for LTCC1 and (d)–(f) for LTCC2, sintered under the same condition of 875°C for 30 min. Inserts show the corresponding selected area electron-diffraction patterns and EDS patterns.

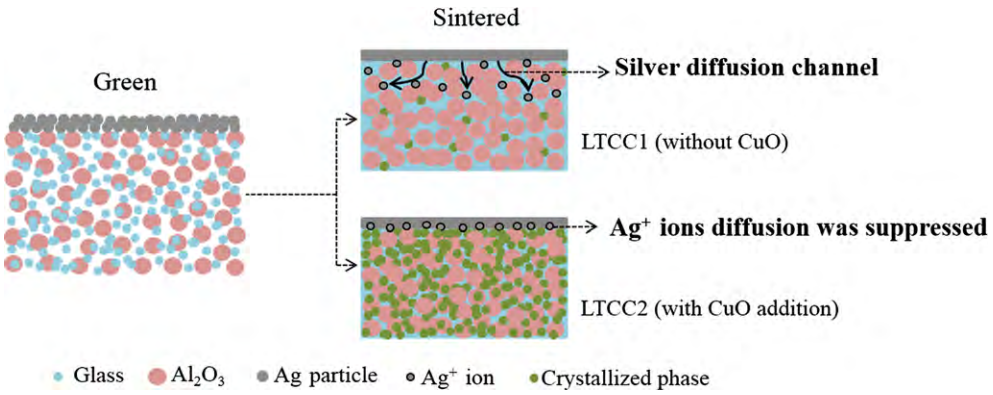

Fig. 8. Schematic diagram of suppressing silver diffusion mechanism in LTCC.

the anorthite phase appears more obvious in Figs. 7(d) and (e) compared with Figs. 7(a)–(c). The SAED pattern of the region with fringes shown in Fig. 7(e) reveals that these regions are composed of triclinic anorthite crystallized from glass matrix. The crystallization character of LTCC2 could be further demonstrated by the high-resolution transmission electron microscopy image as shown in Fig. 7(f). The crystalline lattice can be clearly seen. The interplanar distance is about 0.34 nm, which is corresponding to the (−1 1 4) plane of anorthite (PDF Standard 41-1486).

In addition to the different crystallinity, the particles with high-contrast in the glass matrix are observed in Figs. 7(a)–(c), which are indicated by the arrows. These particles can be observed more obvious in the dark field image of Fig. 7(c). According to the analysis of energy dispersive spectra (EDS) on the marked areas of 1 and 2, these particles are very likely to be silver particles. It was worth to mention that these particles are unstable during the TEM observations. They could move and melt in the glass matrix when irradiated by the high-energy electron beam. The high-energy irradiation during TEM operation can produce electron-hole pairs which individually become trapped at various defect sites in the glass structure.[24] Due to Ag^+ is a strong electron trapper, the reduction in silver could be induced in the high vacuum environment of TEM operation:

$$Ag^+ + e^- \rightarrow Ag^0$$

Figure 8 shows a schematic diagram of silver diffusion mechanism in the borosilicate glass-based LTCC materials. As glass network modifier, Ag^+ ions are very likely to migrate into LTCC materials through the glass network

during cofiring process. The addition of CuO can greatly promote the crystallization of glass matrix of the LTCC material. Therefore, the diffusion activation energy of Ag^+ ions increases dramatically and silver diffusion may be suppressed.[25] Furthermore, the crystallization of the glass matrix could block the Ag^+ ions diffusion channel.

IV. Conclusions

The silver diffusion behavior in the LTCC materials comprised of alumina and borosilicate glass was investigated. XPS and TEM analysis indicated that silver ions diffused into LTCC materials through the glass phase. The CuO additive in glass compositions enhanced the crystallization of glass matrix of the LTCC materials. The enhancement in crystallization of the glass matrix induced the reduction in the diffusion coefficient and the increase in diffusion activation energy of silver ions. As a result, the diffusion of silver ions during the cofiring process was suppressed.

Acknowledgments

The authors acknowledge the financial support from the Chinese National Natural Science Foundation (grant no. 61371060, 61501438), the Ministry of Science and Technology of China through 863-Project (2015AA034102), and M. S. Ma was supported by Shanghai Sailing Program (grant no. 15YF1413700).

References

[1]R. R. Tummala, "Ceramic and Glass-Ceramic Packaging in the 1990s," *J. Am. Ceram. Soc.*, **74**, 895–908 (1991).

[2]J. N. Calata, J. G. Bai, X. Liu, S. Wen, and G. Q. Lu, "Three-Dimensional Packaging for Power Semiconductor Devices and Modules," *IEEE Trans. Adv. Packag.*, **28**, 404–12 (2005).

[3]M. T. Sebastian1 and H. Jantunen, "Low Loss Dielectric Materials for LTCC Applications: A Review," *Int. Mater. Rev.*, **53**, 57–90 (2008).

[4]Y. Imanaka, *Multilayered Low Temperature Cofired Ceramics (LTCC) Technology, Part 1*. Springer, Boston, MA, 2005.

[5]X. M. Cui, B. Li, J. H. Shen, Y. H. Wang, and J. Zhou, "The Co-Fired Behaviors Between Ag and Glass–Ceramics Materials in LTCC," *J. Electroceram.*, **21**, 541–4 (2008).

[6]Y. F. Zhang, S. L. Bai, M. Miao, and Y. F. Jin, "Microstructure and Mechanical Properties of an Alumina-Glass Low Temperature Co-Fired Ceramic," *J. Eur. Ceram. Soc.*, **29**, 1077–82 (2009).

[7]Y. T. Shih, J. H. Jean, and S. C. Lin, "Failure Mechanism of a Low-Temperature-Cofired Ceramic Capacitor with an Inner Ag Electrode," *J. Am. Ceram. Soc.*, **93**, 3278–83 (2010).

[8]J. H. Jean and C. R. Chang, "Interfacial Reaction Kinetics Between Silver and Ceramic-Filled Glass Substrate," *J. Am. Ceram. Soc.*, **87**, 1287–93 (2004).

[9]J. H. Jean, C. R. Chang, and C. D. Lei, "Sintering of a Crystallizable $CaO–B_2O_3–SiO_2$ Glass with Silver," *J. Am. Ceram. Soc.*, **87**, 1244–9 (2004).

[10]K. B. Shim, N. T. Cho, and S. W. Lee, "Silver Diffusion and Microstructure in LTCC Multilayer Couplers for High Frequency Applications," *J. Mater. Sci.*, **35**, 813–20 (2000).

[11]M. Prudenziati, B. Morten, A. F. Gualtieri, and M. Leoni, "Dissolution Kinetics and Diffusivity of Silver in Glassy Layers for Hybrid Microelectronics," *J. Mater. Sci. – Mater. Electron*, **15**, 447–53 (2004).

[12]C. S. His, Y. R. Chen, and H. I. Hsiang, "Diffusivity of Silver Ions in the Low Temperature Co-Fired Ceramic (LTCC) Substrates," *J. Mater. Sci.*, **46**, 4695–700 (2011).

[13]M. Valant and D. Suvorov, "Chemical Compatibility Between Silver Electrodes and Low-Firing Binary-Oxide Compounds: Conceptual Study," *J. Am. Ceram. Soc.*, **83**, 2721–9 (2000).

[14]D. W. Kim, K. H. Ko, and K. S. Hong, "Influence of Copper(II) Oxide Additions to Zinc Niobate Microwave Ceramics on Sintering Temperature and Dielectric Properties," *J. Am. Ceram. Soc.*, **84**, 1286–90 (2001).

[15]S. Q. Yu, B. Tang, X. Zhang, S. R. Zhang, and X. H. Zhou, "Improved High-Q Microwave Dielectric Ceramics in CuO-Doped $BaTi_4O_9–BaZn_2Ti_4O_{11}$ System," *J. Am. Ceram. Soc.*, **95**, 1939–43 (2012).

[16]M. S. Ma, Z. F. Liu, Y. X. Li, Y. P. Zeng, and D. X. Yao, "Enhanced Thermal Conductivity of Low-Temperature Sintered Borosilicate Glass-AlN Composites with β-Si_3N_4 Whiskers," *J. Eur. Ceram. Soc.*, **33**, 833–9 (2013).

[17]Z. F. Liu, Y. L. Wang, and Y. X. Li, "Combinatorial Study of Ceramic Tape-Casting Slurries," *ACS Comb. Sci.*, **14**, 205–10 (2012).

[18]A. V. Naumkin, A. Kraut-Vass, S. W. Gaarenstroom, and C. J. Powell, NIST X-ray Photoelectron Spectroscopy Database 20, Version 4.1. http://srdata.nist.gov/xps/Default.aspx. Last accessed on September 15, 2012.

[19]G. I. N. Waterhouse, G. A. Bowmaker, and J. B. Metson, "Interaction of a Polycrystalline Silver Powder with Ozone," *Surf. Interface Anal.*, **33**, 401–9 (2002).

[20]G. B. Hoflund and Z. F. Hazos, "Surface Characterization Study of Ag, AgO, and Ag_2O Using X-ray Photoelectron Spectroscopy and Electron Energy-Loss Spectroscopy," *Phys. Rev. B*, **62**, 11126–33 (2000).

[21]K. Masuko, "Glass-Ceramic Composition for Ceramic Electronic Part, Ceramic Electronic Part, and Method for Manufacturing Multilayer Ceramic Electronic Part"; US Patent No. 6667256, 2003.

[22]A. Panacek, L. Kvitek, R. Prucek, M. Kolar, R. Vecerova, et al., "Silver Colloid Nanoparticles: Synthesis, Characterization, and Their Antibacterial Activity," *J. Phys. Chem. B*, **110**, 16248–53 (2006).

[23]R. Müller, R. Meszaros, B. Peplinski, S. Reinsch, M. Eberstein, and W. A. Schiller, "Dissolution of Alumina, Sintering, and Crystallization in Glass Ceramic Composites for LTCC," *J. Am. Ceram. Soc.*, **92**, 1703–8 (2009).

[24]J. W. Sheng, "Photo-Induced and Controlled Synthesis of Silver Nanocluster in Soda-Lime Silicate Glass," *Int. J. Hydrogen Energy*, **32**, 2602–5 (2007).

[25]F. Mezei and W. Knaak, "Neutron Spin Echo Study of Dynamic Correlations Near Liquid-Glass Transition," *Phys. Scripta*, **19**, 363–8 (1987). □